THE LANCET
Diabetes & Endocrinology

Supplementary appendix

This appendix formed part of the original submission. We post it as supplied by the authors.

Supplement to: Kanczkowski W, Evert K, Stadtmüller M, et al. COVID-19 targets human adrenal glands. *Lancet Diabetes Endocrinol* 2021; published online Nov 18. http://dx.doi.org/10.1016/S2213-8587(21)00291-6.

Supplementary appendix: COVID-19 targets human adrenal glands.

Supplementary Appendix - Table of contents: Page:

Material and Methods

Adrenal tissue samples

Formalin-Fixed Paraffin-Embedded (FFPE) adrenal gland tissue sections from autopsies of patients who died of COVID-19 (COVID-19 patients) and control tissues of patients who died due to causes unrelated to infection (control autopsies) were obtained from the Institute of Pathology at the Universität Regensburg, Institute of Pathology at Universitätsklinikum Carl Gustav Carus in Dresden (Germany) and from Department of Pathology and Molecular Pathology, University Hospital Zurich (Switzerland). Adrenal FFPE tissue sections from COVID-19 patients collected in Dresden and Regensburg were received through the German Registry for COVID-19 Autopsies (DeRegCovid). Ethics Committees in Dresden, Regensburg and Zürich were informed of the study and approved it. Written consents from relatives of all deceased patients have been received. Clinical information is provided in table 1 (appendix p 1). In this study, we have analyzed all available adrenal tissues from patients with COVID-19 (40 cases), which precludes a potential selection bias. These tissues were collected from autopsies performed during the COVID-19 pandemic between March 2020 and March 2021. All forty patients who died because of COVID-19 had a SARS-CoV-2 infection confirmed by positive pharyngeal swabs (RT-qPCR). Seven control adrenal gland tissues used in this study were obtained from autopsies of patients who died between January 2012 and February 2020 (before the COVID-19 pandemic). Post mortem, control tissues were chosen based on tissue availability and time of autopsy. Control and COVID-19 patients were not matched for age or gender.

Human adrenal and kidney paraffin sections were purchased from Zyagen (San Diego, CA, USA). Adrenal proteins were isolated from adult adrenal tissues resected during tumour nephrectomy, which was approved by the ethical committee of the Medical Faculty of the Technical University Dresden (Approval Nr. EK219102004). Experienced pathologists verified normal histological appearance of sections obtained from those tissues.

Supplementary Table 1. Patients' characteristics.

	Age	Sex	Cause of Death	Comorbidity	BMI	Glucocorticoids
COVID-19 Patient 1	68	f	Septic MOF	Hypertension, obesity	35·4	No
COVID-19 Patient 2	73	m	Septic MOF	Hypertension, COPD	26·2	Dexamethasone
COVID-19 Patient 3	44	f	Septic MOF	Obesity	40·4	Dexamethasone
COVID-19 Patient 4	61	f	Respiratory MOF	Liver cirrhosis	20·8	No

COVID-19 Patient 5	51	m	Septic MOF	None	29·2	Dexamethasone
COVID-19 Patient 6	68	m	Septic MOF	Hypertension, obesity, DM	34·0	Dexamethasone
COVID-19 Patient 7	65	m	Septic MOF	Hypertension	27·8	No
COVID-19 Patient 8	64	f	Respiratory MOF	Hypertension	27·7	Dexamethasone
COVID-19 Patient 9	68	m	Septic MOF	Influenza	24·7	Dexamethasone
COVID-19 Patient 10	45	f	Unknown	Obesity, DM	51·0	Dexamethasone
COVID-19 Patient 11	55	m	Bronchopneumonia	Hypertension, obesity	31·4	Dexamethasone
COVID-19 Patient 12	71	f	ARDS, sepsis	Asthma bronchiole	17·6	Prednisolon
COVID-19 Patient 13	85	m	ARDS, sepsis	Coronary heart disease, NHL	27·3	No
COVID-19 Patient 14	62	m	Respiratory MOF	Coronary heart disease	28·0	Dexamethasone
COVID-19 Patient 15	67	m	Respiratory MOF	Adiposities	40·8	N/A
COVID-19 Patient 16	79	m	Respiratory MOF, sepsis	Coronary heart disease, pulmonary fibrosis, hypertension	22·2	Dexamethasone
COVID-19 Patient 17	88	f	Respiratory MOF	Hypertension	27·0	Dexamethasone
COVID-19 Patient 18	90	m	Respiratory MOF	Metastatic melanoma	19·8	Dexamethasone
COVID-19 Patient 19	88	m	ARDS	Hypertension, vascular dementia	20·1	No
COVID-19 Patient 20	73	m	Respiratory MOF	Dilative cardiomyopathy	23·0	Dexamethasone
COVID-19 Patient 21	87	f	Sepsis	Renal insufficiency	19·4	No
COVID-19 Patient 22	88	f	ARDS	Obesity	35·0	No
COVID-19 Patient 23	68	m	Sepsis	Metastatic lung carcinoma	27·5	Prednison
COVID-19 Patient 24	84	m	ARDS, sepsis	Coronary heart disease	18·6	Dexamethasone
COVID-19 Patient 25	70	f	ARDS	Metastatic colorectal carcinoma	29·4	Dexamethasone
COVID-19 Patient 26	73	m	ARDS	Coronary heart disease	27·2	Dexamethasone
COVID-19 Patient 27	24	m	Acute cardiac failure, bronchopneumonia	Coronary heart disease	27·8	No
COVID-19 Patient 28	85	m	ARDS	Hypertension	28·4	Unknown
COVID-19 Patient 29	59	f	Bronchopneumonia	DM	28·8	Dexamethasone
COVID-19 Patient 30	80	m	ARDS acute cardiac failure	Coronary heart disease	26·1	No
COVID-19 Patient 31	63	m	Bronchopneumonia, sepsis	Cerebral dementia	19·7	No
COVID-19 Patient 32	80	m	Respiratory MOF	Coronary heart disease, COPD	21·6	Methylprednisolon
COVID-19 Patient 33	62	m	ARDS, systemic thromboembolism	AML	28·4	Dexamethasone
COVID-19 Patient 34	89	m	ARDS with MOF	Coronary heart disease	17·7	Dexamethasone
COVID-19 Patient 35	57	m	ARDS with MOF	Pulmonary fibrosis obesity	34·2	Hydrocortisone
COVID-19 Patient 36	66	f	ARDS with MOF	Liver cirrhosis, obesity	43·6	N/A
COVID-19 Patient 37	74	f	Bronchopneumonia sepsis	Coronary heart disease	29·3	Hydrocortisone

COVID-19 Patient 38	47	m	ARDS	DM	26·1	No
COVID-19 Patient 39	59	f	ARDS with MOF	DM, obesity	37·8	Hydrocortisone
COVID-19 Patient 40	79	f	ARDS	Hypertension	21·6	No
Control Autopsy 1	71	m	Haemorrhagic shock	Yes	Unkn.	Unkn.
Control Autopsy 2	62	m	Cardiogenic shock	Yes	Unkn.	Unkn.
Control Autopsy 3	75	m	Cardiogenic shock	Yes	Unkn.	Unkn.
Control Autopsy 4	84	m	Cardiogenic shock	Yes	Unkn.	Unkn.
Control Autopsy 5	65	f	Cardiogenic shock	Yes	Unkn.	Unkn.
Control Autopsy 6	51	f	COPD	Hypertension	Unkn.	Unkn.
Control Autopsy 7	70	m	Heart attack	Hypertension	Unkn.	Unkn.
Control Autopsy 8	77	m	Pneumonia	Hypertension	Unkn.	Unkn.
Normal Adrenal	Unkn.	Unkn.	N/A	N/A	Unkn.	Unkn.
Normal Kidney	Unkn.	Unkn.	N/A	N/A	Unkn.	Unkn.

Tabular summary of the adrenal gland tissue donor patients including age, sex: female (f) & male (m), cause of death, comorbidities, body mass index (BMI) and use of glucocorticoids. Dex – dexamethasone. DM – Diabetes Mellitus. Data unknown (Unkn.) or Not applicable (N/A). MOF- Multi organ failure. COPD: Chronic Obstructive Pulmonary Disease, NHL: Non-Hodgkin Lymphoma, MOF. Multi-Organ Failure, AML: Acute Myeloid Leukaemia.

Immunohistochemistry/Immunofluorescence

Prior to staining, adrenal FFPE tissue slices were first deparaffinised in Neo-Clear (Merck) and then subsequently rehydrated through a descending series of ethanol. Antigen retrieval was performed in citrate retrieval buffer pH 6·0, using a decloaking Chamber NXGEN (Menarini Diagnostics) at 110°C for 3 minutes (most of antibodies) and for 20 min (in case of GTX 632604 antibody). Tissue slices and cells used for immunofluorescence were fixed in 4% PFA solution for 10 minutes at RT. After washing, sections were immersed in blocking buffer consisting of 2 mg/ml of BSA, 0.1% Triton X-100, 0·15% Glycine and 5% of either goat or donkey serum dissolved in PBS, for 1 hour at room temperature. The immunostaining process was continued by incubation of slides in blocking buffer with the respective primary antibodies at 4°C overnight (table S2, appendix p 3). Slides were washed and incubated with the appropriate fluorophore-conjugated secondary antibodies in PBS for 2 hours at room temperature. Nuclei were stained with Hoechst 33342 (Thermo Fisher Scientific) and slides were mounted with fluorescent mounting medium (AquaPoly/Mount; Polysciences). For immunohistochemistry, deparaffinised FFPE sections were blocked and stained using appropriate antibodies and Vectastain ABC Kit Peroxidase and AEC Substrate Kit for Peroxidase following the instructions of the manufacturer (Vector Laboratories). Immunohistochemical staining presented in Fig. S1 was done with a Ventana Benchmark XT Autostainer as previously described (Varga Z *et al.* 2020). Tissues were counterstained with hematoxylin. Imaging was performed with a Zeiss LSM Airy 880 inverted confocal laser scanning microscope and ZEN 2·3 (black edition) software (Zeiss, Germany) and Axio Imager.M2 Zeiss fluorescence microscope and Zen 2 software (Zen Blue edition). Image processing and analysis were carried out using the ImageJ software (v.1.53c; NIH, USA).

Supplementary Table 2. Antibody characteristics used in this study.

Antibody	**Source**	**Catalog Nr.**	**Dilution/Application**
Goat pAb anti-CgA	Santa Cruz Biotech.	sc1488	1:100 IF
Mouse mAb anti-VCAM-1	Thermo Fisher Scientific	MA5-11447	1:50 IF
Rabbit pAb anti-ACE2	Abcam	ab15348	1:500 IF / 1:1000 WB
Mouse mAb anti-ACE2	Thermo Fisher Scientific	MA5-31394	1:10000 IF / 1:700 WB
Rabbit pAb anti-ACE2	Sigma-Aldrich	HPA000288	1:100 IF / 1:500 WB
Rabbit pAb anti-TMPRSS2	Abcam	ab92323	1:1000 IF / 1:500 WB
Mouse mAb anti-Vimentin	Abcam	ab8978	1:100 IF

Rabbit pAb anti-pMLKL	Abcam	ab187091	1:250 IF
Mouse mAb anti-SARS-CoV-2-N	Santa Cruz Biotechnology	sc65653	1:100 IHC
Mouse mAb anti-SARS-CoV-2-S (1A9)	Gentex	GTX632604	1:500 IF & IHC
Mouse mAb (PG-M1) anti-CD68	DAKO	M0876	1:50 IHC
Rabbit mAb (SP7) anti-CD3e	Thermo Scentific	MA1-90582	1:300 IHC
rabbit pAb-anti-CD31	Abcam Limited	ab28364	1:100 IHC
rabbit mAb (SP35) anti-CD4	Cell Marque Lifescreen	104R-16	1:100 IHC

IF – immunofluorescence, WB – Western blot, IHC – immunohistochemistry, pAB – polyclonal antibodies, mAB – monoclonal antibodies.

Semi-quantitative evaluation of immunohistochemistry of endotheliitis.

Endotheliitis in periglandular fat and in adrenal parenchyma was evaluated based on immunohistochemistry staining and was scored as follows: score 0: absent, score 1+: “mild”, in scattered (<5 per gland) capillaries detected with CD45 immunostaining, score 2+: “moderate”, scattered (<5 per gland) endotheliitis in capillaries or small sized vessels detected with H&E stain, score 3+: “high” numerous (>5 per gland) endotheliitis in capillaries or in small sized vessels.

RNA in-situ hybridisation

RNAscope was performed using the RNAscope® 2·5 High Definition (HD)—BROWN Assay on formalin-fixed paraffin-embedded tissues using a probe against SARS-CoV-2-S (V-nCoV2019-S, cat. No. 848561), and a probe against StAR (Hs-STAR, cat. No. 474551) following the instructions of the manufacturer (ACDBio). Internal assay positive control - peptidylprolyl isomerase B (PPiB) and negative probe targeting bacterial gene dihydrodipicolinate reductase (dapB) were used. Positive signal was developed using the DAB system for a total of 20 min. Tissues were then counterstained with haematoxylin for 30 seconds, washed and subsequently dried at 60°C for 15 min. After cooling at RT, slides were mounted and visualised with a 40x objective on a Axio Imager.M2 Zeiss microscope.

Transmission electron microscopy (TEM)

TEM processing of post mortem tissue was performed as previously described (Völkner *et al.*, 2021). Briefly, FFPE adrenal tissues from SARS-CoV-2 triple positive (ISH, IHC, RT-qPCR) COVID-19 Patients “Case 33” were fixed in 2.5% glutarladehyde in 100 mM phosphate buffer and dissected for further processing. Samples were washed and further postfixed in 2% aqueous OsO4 solution containing 1.5% potassium ferrocyanide and 2mM CaCl2. After washing, samples were incubated in 1% thiocarbohydrazide, washed again, and contrasted in 2% aqueous OsO4 for a second time. Following additional washes, samples were en-bloc contrasted with 1% uranyl acetate/water, washed again in water, dehydrated in a graded ethanol series and infiltrated in the epon substitute EMBed 812. After embedding, samples were cured at 65°C overnight. Semithin sections were cut with a Leica UC6 ultramicrotome and stained with toluidine blue/borax to identify potential regions of interest, followed by ultrathin sectioning using a diamond knife. Sections were collected on formvar-coated slot grids and stained with lead citrate and uranyl acetate, and imaged on a JEOL JEM1400Plus (camera: Ruby, JEOL) running at 80kV acceleration voltage.

Western blotting

Adrenal proteins were extracted using Cell Lysis Buffer (Cell Signalling Technology, Denvers, MA, USA) according to the manufacturer's instructions. Twenty micrograms of adrenal proteins was separated in polyacrylamide gels and electro-transferred onto PVDF membranes. After one-hour incubation in blocking buffer containing 5% skimmed milk dissolved in 1x Tris-buffered saline and Tween 20 (TBS-T) solution, membranes were incubated in the respective primary antibodies (listed in table S1, appendix p 2) overnight at 4°C. After washing in TBST solution, membranes were incubated in HRP-conjugated secondary antibodies for 1 hour. Chemiluminescent signal was developed using Supersignal West Femto Substrate (Thermo-Pierce) and visualized using G:BOX Chemi gel doc system (Syngene, Cambridge, UK).

RNA extraction from FFPE tissues and RT-qPCR-based detection of SARS-CoV-2

RNA extraction from formalin-fixed, paraffin-embedded (FFPE) adrenal glands was performed using a modified, Trizol-based extraction protocol. Briefly, FFPE sections were incubated for 10 min at 95°C in extraction buffer (1 M Tris pH 8·0, 0·5 EDTA pH 8, and 20% SDS in DNase- and RNase-free H2O). Extracts were then centrifuged at maximum speed for 10 min, followed by removal of remnant paraffin. Subsequently, proteinase K (20 mg/ml) was added to the sample, followed by incubation at 55°C for 48h under constant shaking and centrifugation. Then, 750 µl of Trizol LS Reagent (ThermoFisher Scientific) was added to 250 µl of the supernatant and homogenized using QIA-shredder columns for 2 min at maximal speed. After chloroform extraction, the aqueous phase was carefully collected and mixed with 1 µl of glycogen and 500 µl of isopropanol. RNA precipitation was performed for 15 min at RT. After precipitation, the tubes were centrifuged for 20 min at maximal speed followed by a washing step in 1 ml of 75% of ice-cold ethanol. The pellet was dried briefly and eventually dissolved in 30 µl RNase-free H2O.

SARS-CoV-2 was detected by multiplex RT-qPCR with virus-specific CDC N1 (CDC.gov) and Charité E-Sarbeco (Corman *et al*. 2020) primers and probes. Human RNase P gene was additionally amplified as quality control for the extraction method and to exclude the presence of potential PCR-inhibitors. For RT-qPCR, 5 µl of eluted sample RNA were mixed with 1 µl primer-probe mix, 2·5 µl TaqPath 1-Step Multiplex Master Mix (No ROX), and 1·5 µl nuclease-free water. The RT-qPCR was performed using the following conditions: preincubation step (2 min/25°C), a cDNA synthesis step (10 min/53°C), a hold step (2 min/95°C), and subsequently 40 cycles of denaturation (10 s/95°C) and annealing/elongation (30 s/55°C). Nuclease-free water was used as the non-template control. The primer pairs and probes for single and multiplex RT-qPCR are shown in Table S3. All reactions were performed on a QuantStudio 7 Pro (Thermo Fisher) thermocycler.

Supplementary Table 3. Primer pairs- and probe-sequences used for multiplex RTq-PCR.

Name	Sequence:5'->3'	Ref.
CDC N1 FWD	GAC CCC AAA ATC AGC GAA AT	CDC.gov
CDC N1 rev	TCT GGT TAC TGC CAG TTG AAT CTG	
CDC N1 Probe	FAM-ACC CCG CAT TAC GTT TGG TGG ACC-BHQ1	
Charité E-Sarbeco fwd	ACA GGT ACG TTA ATA GTT AAT AGC GT	Corman VM et. Al. 2020
Charité E-Sarbeco rev	ATA TTG CAG CAG TAC GCA CAC A	
Charité E-Sarbeco probe	HEX-ACA CTA GCC ATC CTT ACT GCG CTT CG-BHQ1	
CDC RNase P fwd	AGA TTT GGA CCT GCG AGC	CDC.gov
CDC RNase P rev	GAG CGG CTG TCT CCA CAA GT	
CDC RNase P Probe	Cy5-TTC TGA CCT GAA GGC TCT GCG CG-BHQ2	

Using serial dilutions of synthetic Wu-1 SARS-CoV-2 RNA (Wu-1, Twist Bioscience), the efficacy of SARS-CoV-2 qPCR for E-Serbeco-HEX probe and CDC N1-FAM probe was estimated based on the following equation [-1 + 10(-1/slope)] as 99.25% and 98.19% respectively. The detection limit of the assay was 10 viral copies per reaction. SARS-CoV-2 qPCR was additionally validated on FFPE samples collected from COVID-19 and pre-pandemic patients (control autopsies). The results of RT-qPCR analysis of thirty available tissues (Patients 11-40) are presented in table S4 below.

Supplementary Table 4.
Results of RT-qPCR analysis of SARS-CoV-2 detection in FFPE adrenal gland tissues. UND – undetermined.

	SARS-CoV-2 E#1	Sars-CoV-2 E#2	Sars-CoV-2 N1#1	Sars-CoV-2 N1#2	RNaseP #1	RNaseP #2	RESULT
COVID-19 Patient 11	UND.	UND.	UND.	UND.	29·66	26·28	Negative
COVID-19 Patient 12	UND.	UND.	UND.	UND.	20·88	20·96	Negative
COVID-19 Patient 13	UND.	UND.	UND.	UND.	27·21	27·36	Negative
COVID-19 Patient 14	UND.	UND.	UND.	UND.	27·21	27·36	Negative
COVID-19 Patient 15	UND.	UND.	UND.	UND.	28·41	28·88	Negative
COVID-19 Patient 16	UND.	UND.	UND.	35·21	21·77	22·28	Negative
COVID-19 Patient 17	UND.	UND.	32,82	UND.	25·14	25·31	Negative
COVID-19 Patient 18	31·55	28·69	26·68	25·21	24·35	23·23	Positive
COVID-19 Patient 19	UND.	UND.	33·29	UND.	23·87	23·83	Negative
COVID-19 Patient 20	UND.	UND.	35,88	UND.	24·80	25·00	Negative
COVID-19 Patient 21	UND.	UND.	33·93	33·44	23·79	23·82	Positive
COVID-19 Patient 22	UND.	UND.	30·04	UND.	21,49	22·52	Negative
COVID-19 Patient 23	UND.	UND.	35·03	32·24	29·11	27·83	Positive
COVID-19 Patient 24	29·09	28·86	25·31	25·10	25·24	25·14	Positive
COVID-19 Patient 25	29·09	28·86	25·31	25·10	25·24	25·14	Positive
COVID-19 Patient 26	33·42	30·25	27·05	26·41	29·80	28·28	Positive
COVID-19 Patient 27	UND.	UND.	UND.	34·16	18·73	20·11	Negative
COVID-19 Patient 28	UND.	UND.	UND.	UND.	21·67	26·66	Negative
COVID-19 Patient 29	UND.	35·53	31·37	31·78	22·52	22·55	Positive
COVID-19 Patient 30	UND.	35·53	31·37	31·78	22·52	22·55	Positive
COVID-19 Patient 31	23·46	20·40	20·36	19·24	21·70	21·32	Positive
COVID-19 Patient 32	28·36	26·57	24·77	25·16	21·17	21·02	Positive
COVID-19 Patient 33	UND.	UND.	32·04	29·59	22·27	20·75	Positive
COVID-19 Patient 34	24·01	24·04	20·75	20·75	21·45	21·30	Positive
COVID-19 Patient 35	27·85	27·75	23,34	22·64	21·62	21·66	Positive
COVID-19 Patient 36	30·56	UND.	UND.	UND.	29·98	21·62	Negative
COVID-19 Patient 37	UND.	29·76	26·63	24·34	23·86	22·28	Positive

COVID-19 Patient 38	UND.	29·76	26·63	24·34	23·86	22·28	Positive
COVID-19 Patient 39	UND.	UND.	UND.	UND.	30·01	30·20	Negative
COVID-19 Patient 40	UND.	UND.	UND.	UND.	30·01	29·85	Negative

In vitro SARS-CoV-2 infection

Human adrenocortical carcinoma cells (NCI-H295R) were grown on glass slides until 70% of confluence was reached. Infection with SARS-CoV-2 Virus "hCoV-19/Germany/SN-RKI-I-038776/2021 (B.1.1.7/Alpha)" at MOI 5 was performed in PBS supplemented with 0.3 % bovine albumin and 1 mM $MgCl_2$ and 1 mM $CaCl_2$. Mock-infected control cells were incubated in the same medium but without virus. After 1 h incubation at 37°C and 5% CO_2 with occasional shaking, the inoculum was removed and the unbound virus removed by washing with PBS. Cells were supplemented with medium (DMEM/F12 supplemented with 10% FBS, 1% penicillin/streptomycin and 1% insulin/transferrin/selenite) and incubated at 37°C and 5% CO_2 for 24 h. The medium was removed and the cells were washed with PBS, followed by fixation and virus inactivation with 4 % formaldehyde for 20 min. Residual formaldehyde was removed by washing with PBS three times. Slides were stored in PBS at 4°C until staining.

Supplementary Table 5.
Summary of SARS-CoV-2 detection in FFPE adrenal gland tissues of patients with COVID-19 by three different methods. ND – not determined.

COVID-19 Patients	IHC	ISH (RNA Scope)	RT-qPCR
Case 1	Positive	Positive	N.D.
Case 2	Negative	Negative	N.D.
Case 3	Positive	Positive	N.D.
Case 4	Negative	Negative	N.D.
Case 5	Positive	Positive	N.D.
Case 6	Positive	Positive	N.D.
Case 7	Negative	Positive	N.D.
Case 8	Negative	Negative	N.D.
Case 9	Negative	RNA degradation	N.D.
Case 10	Negative	RNA degradation	N.D.
Case 11	Positive	Positive	Negative
Case 12	Negative	Negative	Negative
Case 13	Positive	Positive	Negative
Case 14	Negative	Negative	Negative
Case 15	Negative	Negative	Negative
Case 16	Negative	Negative	Negative
Case 17	Positive	Positive	Negative
Case 18	Negative	Negative	Positive
Case 19	Positive	Positive	Negative
Case 20	Negative	Negative	Negative
Case 21	Positive	Positive	Positive
Case 22	Positive	Positive	Negative
Case 23	Positive	Negative	Positive

Case 24	Positive	Positive	Positive
Case 25	Negative	Negative	Positive
Case 26	Negative	Negative	Positive
Case 27	Negative	Negative	Negative
Case 28	Positive	Positive	Negative
Case 29	Negative	Negative	Positive
Case 30	Positive	Positive	Positive
Case 31	Positive	Positive	Positive
Case 32	Positive	Positive	Positive
Case 33	Positive	Positive	Positive
Case 34	Negative	Negative	Positive
Case 35	Positive	Positive	Positive
Case 36	Negative	Negative	Negative
Case 37	Negative	Negative	Positive
Case 38	Negative	Negative	Positive
Case 39	Negative	Negative	Negative
Case 40	Negative	Negative	Negative

Data availability and sharing

The authors declare that the data supporting the findings of this study are available within the paper. Individual participant data reported in this study can only by shared upon justified request addressed to the corresponding author.

Contributors

WK, MS, MH, LL, LSC, KE and ZV – data curation; WK, LSC, SRB – conceptualization; WK, MS, MH, LL, KF, KE, ZV – formal analysis; JP, SG, AA, ZV – resources; WK, ZV, SRB –writing, review and editing; FB, SRB – supervision; CH – funding acquisition. All authors read and approved the manuscript. ZV, WK and SRB have accessed and verified the underlying data. WK and SRB are responsible for the decision to submit the manuscript.

Acknowledgements.

This work was supported by the Deutsche Forschungsgemeinschaft (DFG, German Research foundation) project no. 314061271, TRR 205/1: "The Adrenal: Central Relay in Health and Disease". The work received funding from the German Research Foundation (DFG) to C.H. (HA 8297/1-1). We are grateful to Maria Schuster, Linda Friedrich and Uta Lehnert for performing immunohistochemistry and *in-situ* hybridisation.

Role of the funding source

The funder of the study had no role in study design, data collection, data analysis, data interpretation, or writing of the report.

Supplementary Figures

In our study, we have detected strong and clear ACE2 and TMPRSS2 staining in human normal kidney tissue by immunofluorescence (figure S4A), and found their consistent protein expression in three different human adrenal glands by western blot (figure S4C). Using these antibodies, we have confirmed previously reported expression of both entry factors in VCAM-1 positive adrenal vascular cells and in stromal cells (Hikmet *et al*. 2020). In addition, we have demonstrated TMPRSS2 staining in the adrenocortical cells. Slight background staining was noted in the negative control, which represents a basal autofluorescent signal of adrenal tissue and in particular red blood cells. Furthermore, we have identified for the first time expression of a short isoform of ACE2 (sACE2) in human adrenal protein extracts by western blot (figure S4C) and confirmed its expression in adrenocortical cells by immunohistochemistry (figure S4E) (Mao *et al.* 2020). Although the functionality of this truncated form of ACE2 has been recently questioned based on results of in vitro studies (Blume C *et al.* 2021), its function in vivo in a more complex tissue microenvironment has not yet been evaluated.

References

1. Vogels CBF, Brito AF, Wyllie AL, *et al.* Analytical sensitivity and efficiency comparisons of SARS-CoV-2 RT-qPCR primer-probe sets. *Nat Microbiol*. 2020;**5**:1299-1305.
2. https://www.cdc.gov/coronavirus/2019-ncov/lab/rt-pcr-panel-primer-probes.html “Accessed on 11.10.2021”.
3. Corman VM, Landt O, Kaiser M *et al*. Detection of 2019 novel coronavirus (2019-nCoV) by real-time RT-PCR. Euro Surveill. 2020;**25**:2000045.
4. Varga Z, Flammer AJ, Steiger P *et al.* Endothelial cell infection and endotheliitis in COVID-19. *Lancet.* 2020;**395**:1417-1418.
5. Hikmet F, Mear L, Edvinsson A, Micke P, Uhlen M, Lindskog C. The protein expression profile of ACE2 in human tissues. *Mol Syst Biol* 2020;**16**:e9610.
6. Mao Y, Xu B, Guan W et al. The Adrenal Cortex, an Underestimated Site of SARS-CoV-2 Infection. *Front Endocrinol (Lausanne)* 2020;**11**:593179.
7. Blume C, Jackson CL, Spalluto CM et al. A novel ACE2 isoform is expressed in human respiratory epithelia and is upregulated in response to interferons and RNA respiratory virus infection. *Nat Genet* 2021;**53**:205-214.
8. Völkner M, Kurth T, Schor J et al. Mouse Retinal Organoid Growth and Maintenance in Longer-Term Culture. *Front Cell Dev Biol.* 2021;**9**:645704.

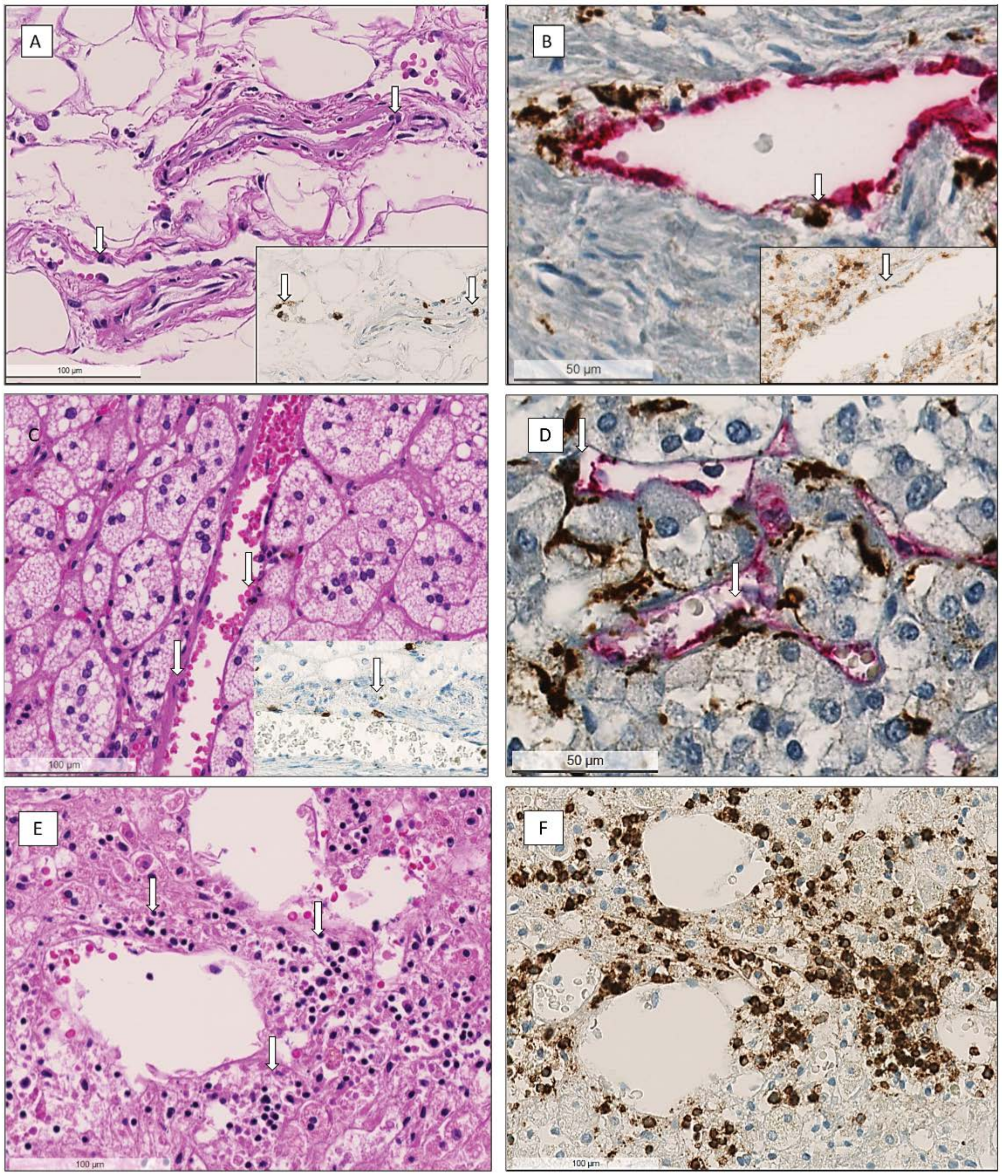

Supplementary Figure 1. Pathological changes found in the human adrenal glands of patients with COVID-19. (A) Morphological appearance of a periglandular venule and arteriole with numerous lymphocytes beneath the endothelial cells (arrows) (hematoxylin & eosin stain). Insert represents scattered CD45-positive lymphocytes in subendothelial location (arrows) (CD45-DAB immunohistochemistry). (B) Small venous vessel endotheliitis in periglandular tissue showing occasional macrophages in subendothelial locations (arrow) (double stain: pink: CD31, brown CD68). Insert represents scattered CD4 positive lymphocytes in subendothelial (arrow) location (CD4-DAB immunohistochemistry). (C) Endotheliitis in the vessels of the adrenal gland showing numerous lymphocytes (arrows) beneath endothelial cells (H&E stain). Insert shows CD45 positive lymphocytes (arrows) beneath endothelial cells. (D) Endotheliitis of a small venous vessel in adrenal gland parenchyma showing occasional macrophages in subendothelial locations (arrow) (double stain: pink: CD31, brown CD68). (E) Perivascular chronic inflammation in the adrenal gland appearing as dissolute or clustered cell population (arrows; H&E stain). (F) Illustration of perivascular chronic inflammation in the adrenal gland. CD45 immunohistochemistry (brown DAB signal) showing abundant perivascular lymphocytes. The tissue was counterstained with haematoxylin. Scale bars represent 100 µm (subpanels A, C, E-F) and 50 µm (subpanels B and D).

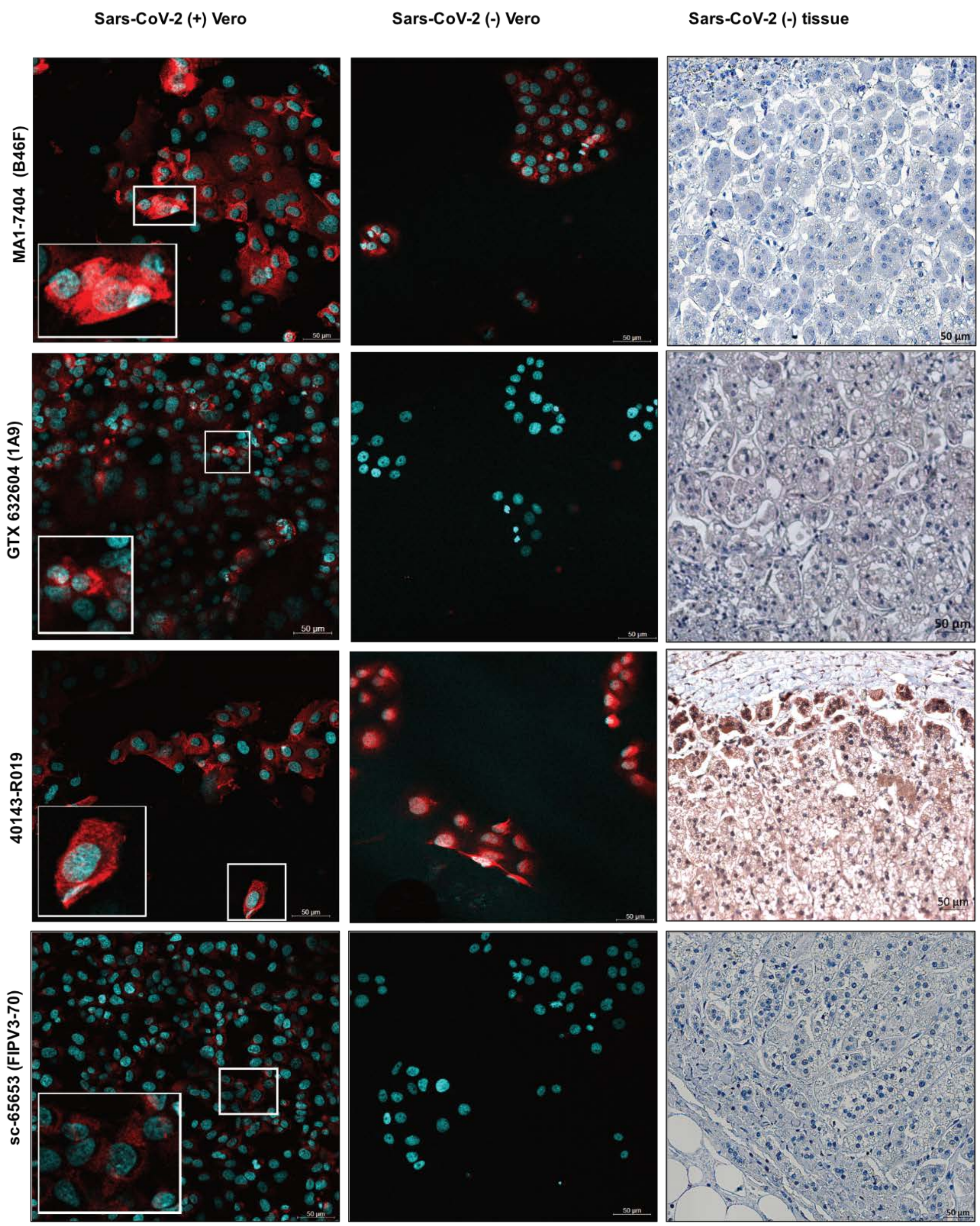

Supplementary Figure 2. Validation of antibodies used for SARS-CoV-2 detection. Four different antibodies were used to detect SARS-CoV-2 in either virus-infected "SARS-CoV-2 (+) Vero" or mock-infected (SARS-CoV-2 (-) Vero) Vero cells. Despite positive signals seen in the case of all four antibodies, two of them gave also unspecific signals in virus-free mock-transfected cells (40143-R019 & MA1-7404), and one (40143-R019) has shown high background in virus-negative adrenal gland tissue "SARS-CoV-2 (-) tissue" collected during an autopsy performed before COVID-19 pandemic. The first two panels represent fluorescent staining (red signal) and the third panel shows immunohistochemical detection (brown DAB signal). The tissue was counterstained with hematoxylin. Scale bars represent 50 μm.

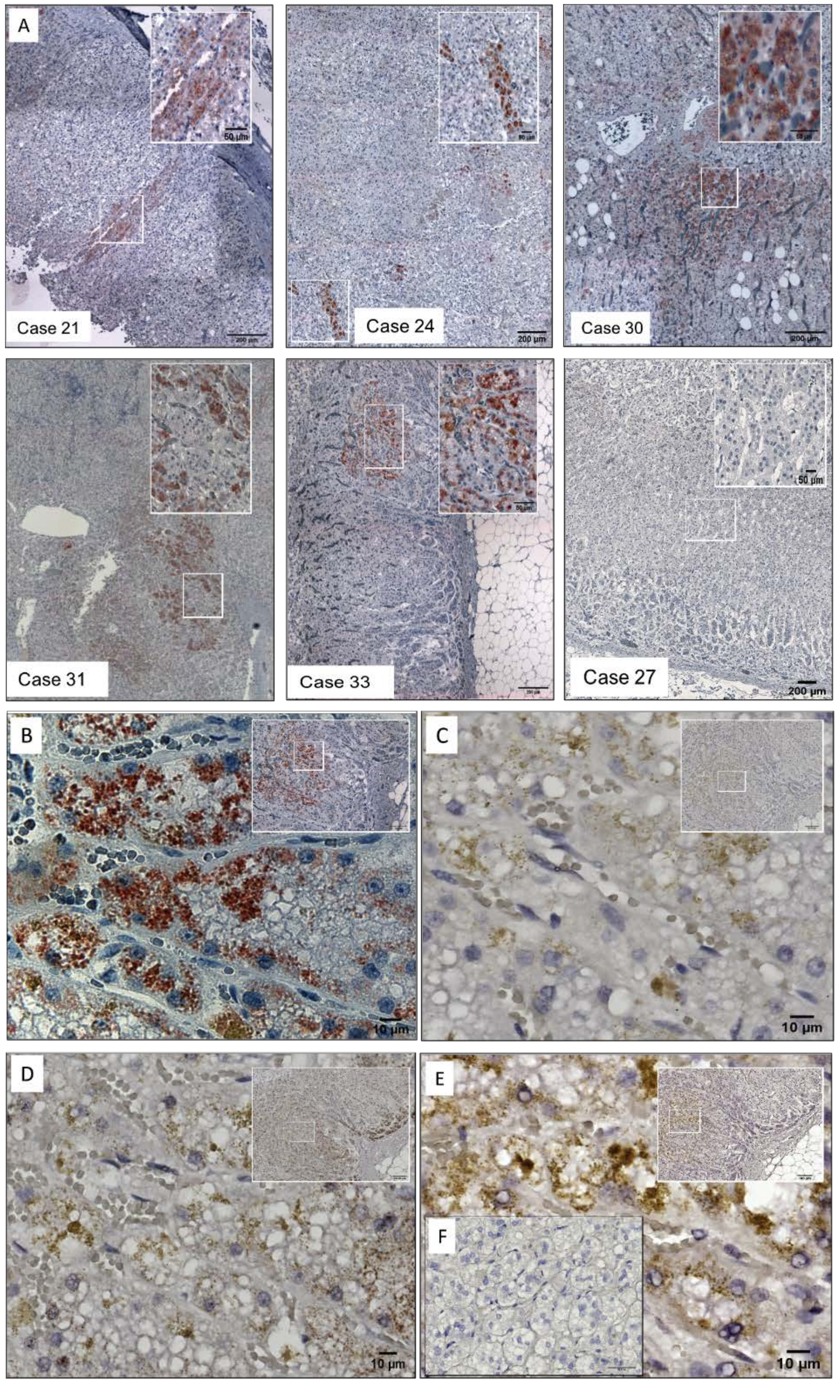

Supplementary Figure 3. Human adrenal glands as targets of COVID-19. (A) Immunohistochemical detection of SIRS-CoV-2 spike protein (red AEC staining) showing diverse staining patterns (from score 2 – case 30, 31 to score 0 “none” – case 27) in case of in adrenal glands of six different patients (COVID-19 cases). Pictures in the upper right corners are magnified regions of interest marked by a white square. Chosen region of interest from COVID-19 patient (case 33) showing SARS-CoV-2 spike protein expression (red AEC signal), which region was then further compared with results of in-situ hybridization performed in subsequent serial 1 mm-thick tissue sections. (C) RNAScope (ISH) detection of RNA encoding for (C) SARS-CoV-2 spike, (D) steroid acute regulatory protein (StAR), and (E) Peptidylprolyl Isomerase B (PPiB) (positive control) in the same region showing spike protein positivity. A clear intracellular RNA hybridization was observed in the case of all three RNA-probes (DAB-brown signal). (F) In contrast, no amplification was found using a probe targeting bacterial gene dihydrodipicolinate reductase (used as a negative control). The tissue was counterstained with hematoxylin. Scale bars from panel A represent 200 µm (50 µm in the insert images). Scale bars from panels B-E represent 10 µm (100 µm in the insert images). The Scale bar in panel F represents 50 µm.

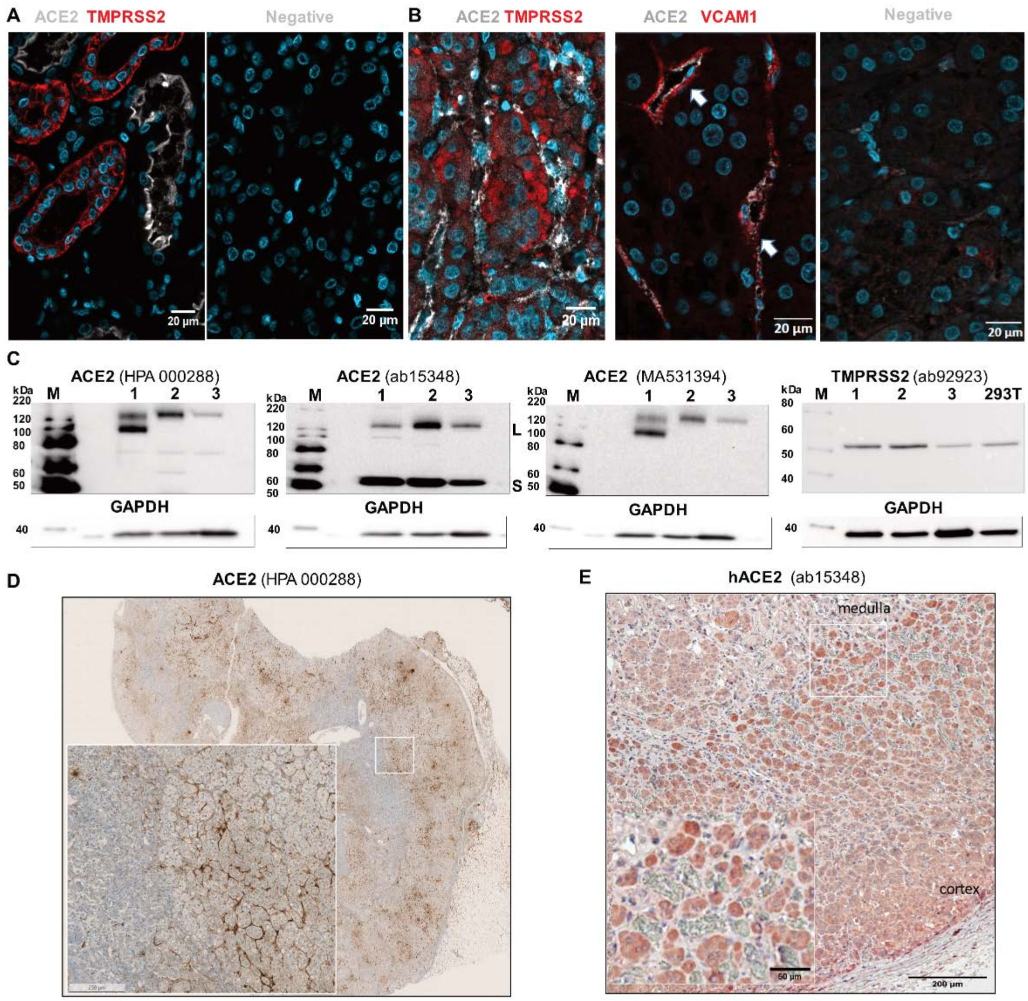

Supplementary Figure 4. Human adrenal glands express receptors for SARS-CoV-2. (A) Angiotensin-converting enzyme 2 (ACE2) receptor in white colour and Transmembrane Serine Protease 2 (TMPRSS2) expression shown in red signal in human kidney tissue (positive control). A strong signal was observed in the distal convoluted tubule but not in the kidney nephron. No colocalization was seen between ACE2 and TMPRSS2. (B) ACE2 was detected in vascular cells expressing vascular adhesion molecule 1 (Vcam-1) but not in adjacent hormone-producing cells. (C) Using western blot, high ACE2 (100-120 kDa) and TMPRSS2 (55 kDa) expression was detected in three normal human adrenal glands (donors) examined. An antibody directed against C-terminal fragment of ACE2 (ab15348) gave an additional band at around 52 kDa, corresponding to the shorter form of ACE2 (S – Short ACE2 and L- long ACE2). 293T –transformed human embryonic kidney cells. Glyceraldehyde 3-phosphate dehydrogenase (GAPDH) was used as a loading control. (D) An immunohistological staining of ACE2 (brown DAB staining) in the adrenal gland of a patient with COVID-19, with proven SARS-CoV-2 infection, showing vascular and perivascular staining. Insert shows a magnified area of interest marked with a white square. An antibody directed against C-terminal fragment of ACE2 (ab15348) positively stained vascular and steroid cells. Negative staining is a control staining without using a primary antibody. Cell nuclei were counterstained with hematoxylin (immunohistochemistry, D&E) or Hoechst 33342 dye (immunofluorescence, A&B). Scale bars from panels A and B represent 20 µm. Scale bar from an insert picture in panel E represents 250 µm. The scale bar in panel F represents 200 µm. (50 µm in the insert image).

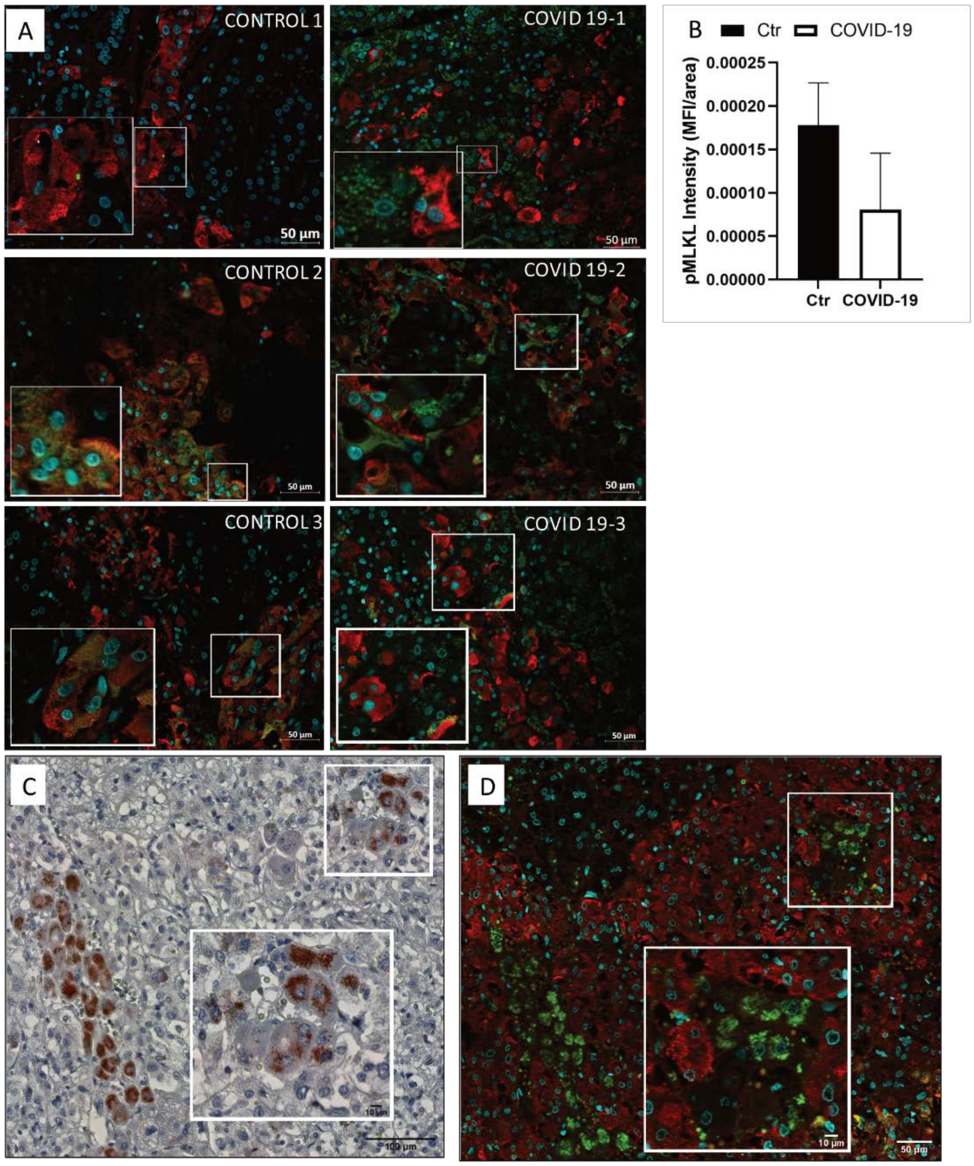

Supplementary Figure 5. COVID-19 is associated with necroptosis of adrenomedullary and adrenocortical cells. (A) Representative pictures of immunofluorescent staining showing expression of phosphorylated mixed lineage kinase domain-like protein (pMLKL) (in green), a marker of activated necroptosis in chromogranin A (CgA)-positive adrenal chromaffin cells (red signal). (B) The mean intensity of fluorescence (MIF) of pMLKL in CgA-positive cells has been analyzed by ImageJ software. No significant difference (Mann-Whitney U-test; p=0·1331) in pMLKL expression was found between adrenal gland samples from COVID-19 patients (n=10) and control patients (n=7) (C) SARS-CoV-2 spike expression in the adrenal gland detected by immunohistochemistry (red AEC signal). (D) In contrast to adrenal medullary cells, expression of pMLKL in the adrenocortical cells was only found in SARS-CoV-2 positive cells. One micrometer (1 µm) -thick serial sections of adrenal gland tissue (COVID-19 case 32) were used in panel C and D. Cell nuclei were counterstained with (C) haematoxylin or with (D) Hoechst 33342. Scale bars in pictures from panel A represent 50 µm, and from panels C-D 100 µm (10 µm in the insert image).